PCCP

PAPER

Cite this: *Phys. Chem. Chem. Phys.*, 2019, **21**, 6207

Structural evolution and electronic properties of $CoSi_n^-$ (n = 3–12) clusters: mass-selected anion photoelectron spectroscopy and quantum chemistry calculations†

Bin Yang,[ab] Xi-Ling Xu,[ab] Hong-Guang Xu,*[ab] Umar Farooq [ac] and Wei-Jun Zheng *[ab]

Received 19th December 2018,
Accepted 19th February 2019

DOI: 10.1039/c8cp07734g

rsc.li/pccp

The structural and electronic properties of cobalt-doped silicon clusters, $CoSi_n^-$ (n = 3–12), are investigated using mass-selected anion photoelectron spectroscopy combined with quantum chemistry calculations. The critical size from an exohedral to an endohedral structure of the anionic clusters is n = 9 and that of the neutral ones is n = 10. Natural population analysis shows transfer of electrons from the silicon framework to the Co atom. The total magnetic moments of $CoSi_3^-$ and $CoSi_4^-$ clusters are 2 μ_B, while those of $CoSi_n^-$ (n = 5–12) clusters are 0 μ_B. The experimental measurements show that $CoSi_{10}^-$ has the highest vertical detachment energy among all the $CoSi_n^-$ (n = 3–12) clusters in the current study. The theoretical calculations show that $CoSi_{10}^-$ has a C_{3v} symmetrical tetracapped trigonal prism structure and very large HOMO–LUMO gap. Both experimental and theoretical results imply that $CoSi_{10}^-$ has unusual stability. Its special stability is attributed to its highly symmetric structure and closed-shell molecular orbital configuration. The structure of neutral $CoSi_{10}$ has relatively lower symmetry as compared to that of $CoSi_{10}^-$ due to Jahn–Teller distortion.

Introduction

Transition metal (TM) doped silicon clusters have been intensively studied by experiments[1–13] and theoretical calculations[14–27] due to their potential applications in the fields of microelectronics, solar cells, and batteries. Cobalt doped silicon clusters have attracted the attention of scientists around the globe, because cobalt-silicide has been widely used as interconnects and metallic contacts in integrated circuit technology.[28] The geometrical and electronic structures of Co atom doped silicon clusters have been investigated previously in several theoretical studies.[29–31] Robles and Khanna studied the structures and magnetic moments of a series of M_2Si_n clusters including Co_2Si_n based on density functional theory calculations.[32] Recently, Li *et al.* investigated neutral $CoSi_n$ (n = 10–12) clusters with tunable IR–UV two-color ionization spectroscopy and density functional theory calculations.[33] They also investigated the structures of $CoSi_n^+$ (n = 5–8) and $Co_2Si_n^+$ (n = 8–12) clusters using infrared multiple photon dissociation spectroscopy and first principles theory study.[34]

Cobalt silicide has a very small lattice mismatch with silicon and shows single crystallinity with epitaxial growth on a substrate.[35–37] It has been reported that $CoSi_2$ is suitable for thin-film silicon-on-insulator technology because of its wide process temperature window and small degradation in scaled devices.[35] Recent studies showed that $CoSi_2$/Si heterostructures at low temperature exhibit an unusually low $1/f$ noise level and, thus, may have potential applications in superconducting quantum interference devices (SQUIDs) and qubits.[36] Investigating the geometrical structures, electronic states, and magnetic properties of cobalt doped silicon clusters may provide useful information for their applications in microelectronics and superconducting devices. To obtain more detailed information about the structural evolution and properties of cobalt–silicon clusters, here, we investigated $CoSi_n^{-/0}$ (n = 3–12) clusters using mass-selected anion photoelectron spectroscopy and quantum chemistry calculations.

Experimental and theoretical methods

Experimental method

The experiments were conducted on a home-built apparatus consisting of a laser vaporization cluster source, a time-of-flight mass spectrometer, and a magnetic-bottle photoelectron

[a] *Beijing National Laboratory for Molecular Sciences, State Key Laboratory of Molecular Reaction Dynamics, Institute of Chemistry, Chinese Academy of Sciences, Beijing 100190, China. E-mail: xuhong@iccas.ac.cn, zhengwj@iccas.ac.cn*

[b] *University of Chinese Academy of Sciences, Beijing 100049, China*

[c] *Department of Chemistry, COMSATS University Islamabad, Abbottabad-Campus, Pakistan*

† Electronic supplementary information (ESI) available. See DOI: 10.1039/c8cp07734g

spectrometer, which has been described elsewhere.[38] The Co–Si cluster anions were generated in the laser vaporization source by laser ablation of a rotating and translating disk target of a mixture of cobalt and isotopically enriched silicon (13 mm diameter, Co : ^{28}Si mole ratio 1 : 4, ^{28}Si 99.989%) with the second harmonic light pulses (532 nm) of a nanosecond Nd:YAG laser (Continuum Surelite II-10). The typical laser power used in this work is about 10 mJ per pulse. Helium gas with a backing pressure of 4 atm was allowed to expand through a pulsed valve (General Valve Series 9) into the source to cool the formed clusters. The generated cluster anions were mass-analyzed with the time-of-flight mass spectrometer. Each $CoSi_n^-$ (n = 3–12) was selected with a mass gate, decelerated by a momentum decelerator, and crossed with the beam of another Nd:YAG laser (Continuum Surelite II-10, 266 nm) in the photodetachment region. The electrons from photodetachment were energy-analyzed through the magnetic-bottle photoelectron spectrometer. The resolution of the magnetic-bottle photoelectron spectrometer was about 40 meV at an electron kinetic energy of 1 eV. The calibration of photoelectron spectra was done with Cu^- and Au^- spectra taken under similar conditions.

Theoretical method

A global search for low-lying structures of $CoSi_n^-$ (n = 3–12) was performed by using CALYPSO software based on a particle swarm optimization algorithm.[39,40] Various low-lying initial structures were randomly generated without symmetry constraints. The Metropolis criterion and bond characterization matrix were incorporated into the method to further enhance the structural evolution and measurement of the structural similarity toward low-energy regions of the potential energy surface. Some structures were retrieved from the literature and used as initial structures. Later, the low-lying isomers were further optimized using the Perdew–Burke–Enzerhof (PBE) functional[41] with Pople's all electron 6-311+G(d) basis set.[42,43] Our previous work confirmed that the PBE functional is suitable for calculating the structures and properties of transition metal doped silicon clusters.[44] To confirm that the structures correspond to true local minima, harmonic vibrational frequencies were calculated. All geometry optimizations were performed without any symmetrical constraints. As a Co atom ($3d^74s^2$) has three unpaired electrons in the valence shell, various spin-multiplicities were considered in order to obtain the lowest energy spin state. In order to obtain more accurate relative energies, the single-point energies of $CoSi_n^-$ (n = 3–12) were calculated by using the coupled-cluster single and double, and perturbative triple excitation (CCSD(T)) method[45,46] with the aug-cc-pVTZ basis set[47] for the Co atoms and the cc-pVDZ basis set[48] for the Si atoms. Zero-point vibrational energy corrections were included for the relative energies of isomers. All theoretical calculations were conducted with the Gaussian 09 program package.[49] The evaluation of spin magnetic moments, atomic charges, and electronic configurations was done through natural bond analysis with the natural bond orbital (NBO) version 3.1 program[50–57] implemented in the Gaussian 09 package, which was also carried out at the PBE/6-311+G(d) level.

Experimental results

The photoelectron spectra of $CoSi_n^-$ (n = 3–12) recorded with 266 nm photons are shown in Fig. 1. The experimental vertical detachment energies (VDEs) and adiabatic detachment energies (ADEs) of $CoSi_n^-$ (n = 3–12) cluster anions obtained from the photoelectron spectra are summarized in Table 1. The VDEs of $CoSi_n^-$ (n = 3–12) are evaluated from the maxima of the first peaks of the photoelectron spectra, and the ADEs are determined by drawing a straight line along the leading edge of the first peak to cross the baseline of the spectra and adding the instrument resolution to the electron binding energy (EBE) values at the crossing points.

As shown in Fig. 1, the spectrum of $CoSi_3^-$ has a peak centered at 2.03 eV followed by a broad band with multiple small peaks centered at 2.76, 3.10, 3.42, 3.64, and 4.03 eV. In addition, an onset of a large peak higher than 4.30 eV is detected in the spectrum. In the spectrum of $CoSi_4^-$, there are three peaks centered at 2.16, 3.05, and 3.73 eV, with a shoulder at about 3.33 eV. With respect to $CoSi_5^-$, it has a peak centered at 2.72 eV and a small low binding energy shoulder centered at 2.45 eV, followed by three unresolved peaks at 3.42, 3.77, and 4.13 eV. The spectrum of $CoSi_6^-$ shows five peaks centered at 2.88, 3.20, 3.39, 3.76, and 4.29 eV. Similarly, two intense peaks centered at 2.94 and 4.11 eV, and a small peak centered at 3.37 eV are observed in the spectrum of $CoSi_7^-$. The $CoSi_8^-$ spectrum has three discernible peaks centered at 3.45, 3.91, and 4.21 eV. The spectrum of $CoSi_9^-$ shows three barely resolved peaks centered at 3.77, 4.11 and 4.30 eV. The spectrum of $CoSi_{10}^-$

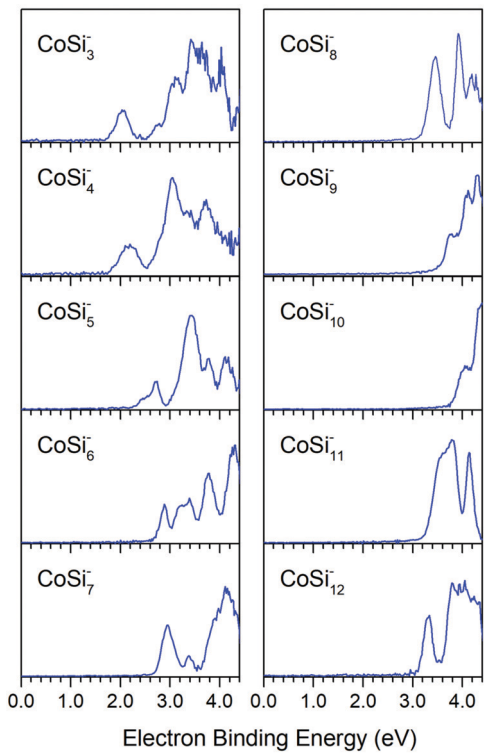

Fig. 1 Photoelectron spectra of $CoSi_n^-$ (n = 3–12) clusters recorded with 266 nm photons.

Table 1 Relative energies, and theoretical VDEs and ADEs of the low-lying isomers of $CoSi_n^-$ (n = 3–12) clusters, and experimental VDEs and ADEs estimated from their photoelectron spectra. The isomers labeled in bold are the most probable isomers in the experiments

Isomer		State	Sym.	ΔE^a (eV)	VDE (eV)		ADE (eV)		Isomer		State	Sym.	ΔE^a (eV)	VDE (eV)		ADE (eV)	
					Theo.[b]	Expt.[c]	Theo.[b]	Expt.[c]						Theo.[b]	Expt.[c]	Theo.[b]	Expt.[c]
$CoSi_3^-$	**3A**	$^3B_1$	C_{2v}	0.00	2.04	2.03	1.89	1.76	$CoSi_8^-$	**8A**	$^1A'$	C_s	0.00	3.26	3.45	3.04	3.19
	3B	$^3A_1$	C_{3v}	0.41	1.69		1.69			8B	$^1A_1$	C_{2v}	0.24	3.12		2.95	
	3C	$^5A'$	C_s	1.01	1.85		1.60			8C	$^1A_1$	C_{2v}	0.32	3.15		2.98	
										8D	$^1A'$	C_s	1.02	3.41		3.25	
$CoSi_4^-$	**4A**	$^3A''$	C_s	0.00	2.27	2.16	2.08	1.82	$CoSi_9^-$	**9A**	$^1A_1$	C_{2v}	0.00	3.65	3.77	3.56	3.56
	4B	$^1A_1$	C_{2v}	0.10	2.02		1.98			9B	^1A	C_1	0.30	3.33		3.01	
	4C	^1A	C_1	0.14	2.40		2.24			9C	$^1A'$	C_s	0.32	3.34		3.17	
	4D	^3A	C_1	0.34	2.33		1.80			9D	$^1A'$	C_s	0.51	3.30		3.08	
$CoSi_5^-$	**5A**	$^1A_1$	C_{2v}	0.00	2.89	2.72	2.72	2.52	$CoSi_{10}^-$	**10A**	$^1A_1$	C_{3v}	0.00	4.02	4.03	3.70	3.75
	5B	$^1A_1$	C_{4v}	0.02	2.45	2.45	2.44	2.29		10B	$^1A_1$	C_{3v}	0.64	3.55		3.37	
	5C	$^1A'$	C_s	0.03	2.80		2.24			10C	$^1A'$	D_{5h}	1.13	2.98		2.92	
	5D	$^3A''$	C_s	0.12	2.60		1.80			10D	$^1A_1$	C_{3v}	1.66	3.52		3.32	
$CoSi_6^-$	**6A**	$^1A'$	C_s	0.00	2.79	2.88	2.59	2.70	$CoSi_{11}^-$	**11A**	$^1A_1$	C_{2v}	0.00	3.46	3.56	3.21	3.27
	6B	$^1A'$	C_s	0.16	2.91		2.33			11B	$^1A_1$	C_{5v}	0.29	3.08		2.99	
	6C	$^1A_1$	C_{5v}	0.59	2.74		2.70			11C	$^1A_1$	C_{2v}	0.50	3.12		3.07	
	6D	$^1A_1$	D_{2d}	0.80	3.20		3.10			11D	$^1A'$	C_s	0.60	3.18		3.13	
$CoSi_7^-$	**7A**	$^1A_1$	C_{2v}	0.00	2.98	2.94	2.95	2.72	$CoSi_{12}^-$	**12A**	$^1A_1$	D_{2d}	0.00	3.10	3.31	3.03	3.10
	7B	^1A	C_1	0.00	3.19	3.37	3.06	3.20		12B	$^1A'$	C_s	0.50	3.36		2.98	
	7C	$^1A'$	C_s	0.13	2.97					12C	$^1A'$	C_s	0.50	3.31		3.22	
	7D	$^3A''$	C_s	0.34	2.74					12D	^1A	C_2	1.09	2.89		2.50	

[a] The ΔE values are calculated at the CCSD(T)//aug-cc-pVTZ/Co/cc-pVDZ/Si level of theory. [b] The ADEs and VDEs are calculated at the PBE/6-311+G(d) level of theory. [c] The uncertainties of experimental VDEs and ADEs are ±0.08 eV.

exhibits two partially resolved peaks at 4.03 eV and 4.37 eV. For the spectrum of $CoSi_{11}^-$, two unresolved peaks centered at 3.56 and 3.78 eV, and a sharp peak at 4.13 eV are observed. $CoSi_{12}^-$ has a well-resolved peak at 3.31 eV followed by a broad unresolved feature between 3.79 and 4.34 eV.

Theoretical results

The typical low-lying isomers of $CoSi_n^-$ (n = 3–12) clusters obtained from density functional theory calculations are presented in Fig. 2 with the most stable ones on the left. Their relative energies, and theoretical VDEs and ADEs are summarized and compared with the experimental values in Table 1. We simulated the photoelectron spectra of the low-lying isomers based on theoretically generalized Koopmans' theorem (GKT)[58,59] and compared the simulated spectra with the experimental spectra as given in Fig. 3. In addition, the optimized structures of neutral $CoSi_n$ (n = 3–12) clusters are shown in Fig. 4.

$CoSi_3^-$. The most stable isomer (3A) of $CoSi_3^-$ is a rhombus structure with C_{2v} symmetry. The calculated VDE of isomer 3A (2.04 eV) is in good agreement with the experimental value (2.03 eV). The simulated spectrum can roughly reproduce the peak positions and patterns of the experimental spectrum. The second stable isomer (3B) can be viewed as a tetrahedron with the Co atom capping a Si_3 triangle, and its energy is higher than 3A by 0.41 eV. Isomer 3C has a bent rhombus structure with C_s symmetry, and it is less stable than 3A by 1.01 eV. The calculated VDEs of isomers 3B and 3C are 1.69 and 1.85 eV, respectively, showing deviation from the experimental value. Therefore, isomer 3A is the most likely one detected in our experiments.

$CoSi_4^-$. The lowest-energy isomer (4A) of $CoSi_4^-$ is a distorted square pyramid with the Co atom at the square base while isomer 4B is a trigonal bipyramid with the Co atom located at the middle triangle. The energy difference observed between isomers 4A and 4B is only 0.10 eV, and their theoretical VDEs (2.27 and 2.02 eV) are both in good agreement with the experimental value (2.16 eV). The combination of the simulated spectra of isomers 4A and 4B can fit the experimental spectrum very well. Thus, it is suggested that isomers 4A and 4B coexist in our experiments. Isomers 4C and 4D are fan-shaped structures with the Co atom at different locations. The energies of isomers 4C and 4D are higher than 4A by 0.14 and 0.34 eV, but the calculated VDE (2.40 eV) of 4C deviates from the experimental value. Thereby, the existence of isomers 4C and 4D in the experiments can be ruled out.

$CoSi_5^-$. In the case of $CoSi_5^-$, isomers 5A, 5B, and 5C are nearly degenerate in energy with 5B and 5C higher than 5A by 0.02 and 0.03 eV. Isomer 5A has a C_{2v} symmetrical structure consisting of a rhombus and a triangle sharing a Co atom. Isomer 5B has a square bipyramid shape with the Co atom at the vertex. Isomer 5C can be seen as a distorted square pyramid with the Co atom at the square base, and the additional Si atom attaches to the Co atom as shown in Fig. 2. Isomer 5D is a distorted trigonal bipyramid with the Co atom located at the vertex, and the fifth Si atom capping on an upper ridge. Isomer 5D is higher in energy than 5A by 0.12 eV. The calculated VDE (2.45 eV) of isomer 5B shows excellent agreement with the experimental value (2.45 eV). The VDE values of isomers 5A, 5C, and 5D are 2.89,

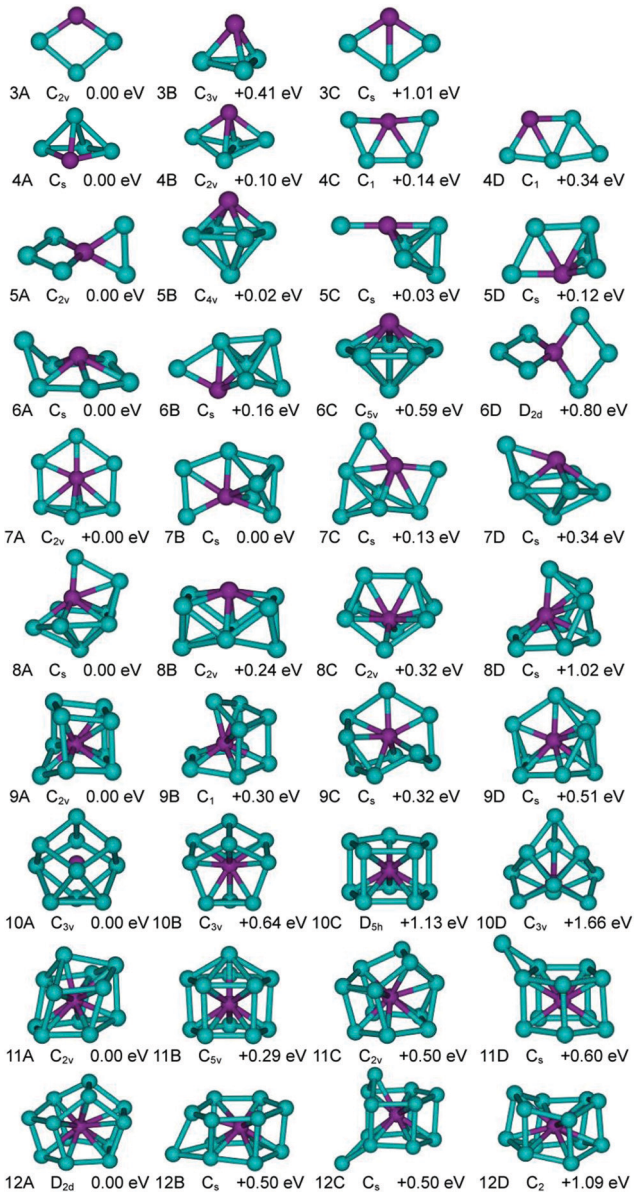

Fig. 2 Typical low-lying isomers of $CoSi_n^-$ (n = 3–12) clusters. The relative energies are calculated at the CCSD(T)//aug-cc-pVTZ/Co/cc-pVDZ/Si level. Purple and cyan balls stand for the Co and Si atoms, respectively.

2.80, and 2.60 eV, comparable to the experimental value (2.72 eV). The combination of the simulated spectra of these four isomers can match the peak positions and patterns of the experimental spectrum. Thus, it is suggested that all these isomers of the $CoSi_5^-$ cluster may exist in our experiments.

$CoSi_6^-$. The most stable isomer (6A) of $CoSi_6^-$ is a pentagonal pyramid with the Co atom located on the vertex, and an additional Si atom attached to one edge of the silicon ring. Isomer 6B can be described as a Si atom capping on one side of a square bipyramid, less stable than 6A in energy by only 0.16 eV. The theoretical VDEs of isomers 6A (2.79 eV) and 6B (2.91 eV) are close to the experimental value (2.88 eV). The combination of the simulated spectra of isomers 6A and 6B could match the peak positions and patterns of the experimental spectrum very well. Isomer 6C is a pentagonal bipyramid with the Co atom located at the vertex. Although the calculated VDE (2.74 eV) of 6C is in good agreement with the experimental one, its energy is still higher than isomer 6A by 0.59 eV. Isomer 6D is less stable than isomer 6A by 0.80 eV. Therefore, the co-existence of isomers 6A and 6B in our experiments has been suggested.

$CoSi_7^-$. The lowest-lying isomer (7A) has the Co atom located at the center of a Si_5 ring with two additional Si atoms symmetrically interacting with one edge of the Si_5 ring. Isomer 7B can be viewed as a distorted tetragonal bipyramid with the Co atom located at the vertex, interacting with a Si_2 dimer. Isomers 7A and 7B are degenerate in energy with 7B higher than 7A by only 0.003 eV. Their calculated VDEs are 2.98 eV and 3.19 eV, respectively. The VDE of isomer 7A is in good agreement with the first peak (2.94 eV) in the experimental spectrum while that of isomer 7B is consistent with the second peak (3.37 eV) in the experimental spectrum. Isomer 7C can be seen as two Si atoms side-capping on a distorted tetragonal bipyramid. Isomer 7D can be constructed by one Si atom face capping on a pentagonal bipyramid with the Co atom located on the vertex. Isomer 7C has a higher energy than 7A by only 0.13 eV, and the theoretical VDE (2.97 eV) of isomer 7C is close to the experimental value too. The combination of the simulated spectra of isomers 7A, 7B and 7C can reproduce the peak positions and patterns of the experimental spectrum. The energy of isomer 7D is higher than isomer 7A by 0.34 eV. The existence of isomer 7D in our experiments is difficult. Therefore, it is suggested that isomers 7A and 7B contribute to the experimental spectrum, and isomer 7C may coexist in our experiments.

$CoSi_8^-$. The most stable isomer (8A) can be viewed as a silicon atom capping a distorted $CoSi_6$ pentagonal bipyramid and an additional silicon atom interacting with the cobalt atom on the upper inclined side. The calculated VDE of isomer 8A (3.26 eV) is close to the experimental value (3.45 eV). The simulated spectrum of isomer 8A can match the peaks and patterns of the experimental spectrum with inconsistent intensities. Isomer 8B can be regarded as a half-endohedral structure with the Co atom located in a boat-shaped Si_8 framework. Isomer 8C shows a handbag-like structure. Similarly, isomer 8D can be viewed as a half-endohedral structure with a tetrahedron cap on the upper inclined side of a Si_5 ring with the Co atom located in the center. The energies of isomers 8B, 8C and 8D are higher than that of isomer 8A by 0.24, 0.32, and 1.02 eV, respectively. Thus, isomer 8A is the most probable one detected in the experiments.

$CoSi_9^-$. As shown in Fig. 2, the lowest-lying isomer (9A) of $CoSi_9^-$ is an endohedral structure with the Co atom encapsulated into a Si_9 cage. The calculated VDE of isomer 9A (3.65 eV) is in good agreement with the experimental value (3.77 eV), and the simulated spectrum reproduces the peak positions, patterns, and intensities in the experimental spectrum very well. Isomers 9B, 9C, and 9D are higher in energy than isomer 9A by 0.30, 0.32, and 0.51 eV, respectively. The calculated VDEs of isomers 9B, 9C, and 9D are 3.33, 3.34, and 3.30 eV, respectively, far from the experimental value (3.77 eV). Thereby, we suggest that only isomer 9A exists in our experiments.

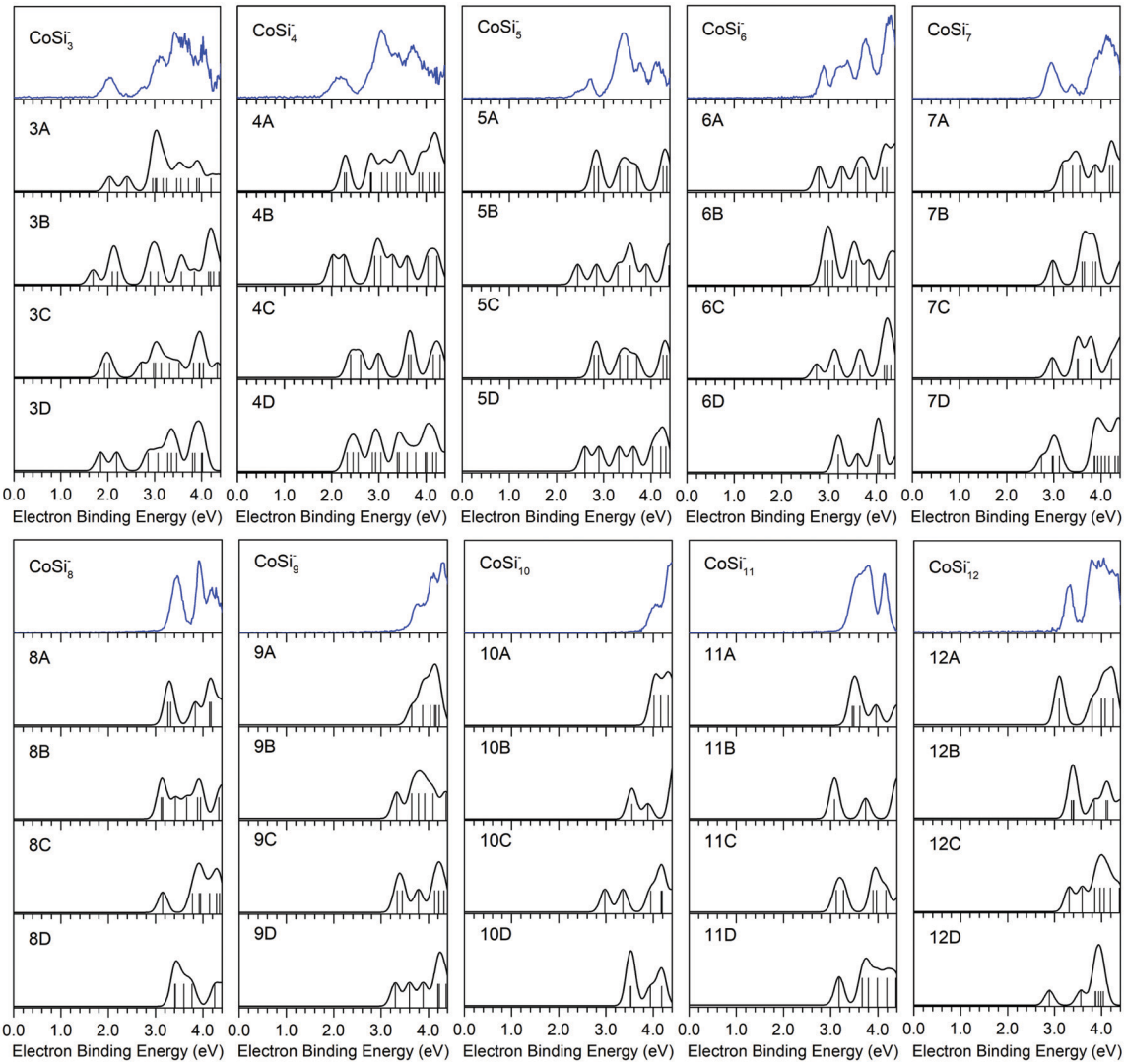

Fig. 3 Comparison between the experimental photoelectron spectra and the simulated spectra of the low-lying isomers of $CoSi_n^-$ (n = 3–12) clusters. Simulated spectra were obtained by fitting the distribution of the transition lines with unit area Gaussian functions of 0.20 eV full width at half maximum.

$CoSi_{10}^-$. In the case of $CoSi_{10}^-$, the most stable isomer (10A) is a tetracapped trigonal prism with C_{3v} symmetry. The Co atom interacts with ten Si atoms and the Co–Si bond lengths are between 2.31 and 2.34 Å, while the Si–Si bond lengths range from 2.46 to 2.62 Å. The theoretical VDE (4.02 eV) is very close to the experimental value (4.03 eV). The simulated spectrum of isomer 10A matches the two peaks (centered at 4.03 and 4.37 eV) of the experimental spectrum very well. Isomer 10B with C_{3v} symmetry is a polyhedron, which has one triangle on the bottom, three quadrangles on the top, and three pentagons on the periphery. Isomer 10C is a pentagonal prism with D_{5h} symmetry, but the open top and open bottom of this pentagonal prism degrade its stability. Isomers 10B, 10C, and 10D are higher in energy than isomer 10A by 0.64, 1.13, and 1.66 eV, respectively. Thereby, isomers 10B, 10C, and 10D can be ruled out and isomer 10A is the most probable one detected in our experiments.

$CoSi_{11}^-$. The most stable isomer 11A of $CoSi_{11}^-$ is a distorted pentagonal prism with one Si face capping on the top. The theoretical VDE of isomer 11A (3.46 eV) is in good agreement with the experimental value (3.56 eV). The simulated spectrum of isomer 11A can match the peak positions and patterns of the experimental spectrum with a difference of the intensities. Isomers 11B, 11C, and 11D are derived from isomer 10C, the pentagonal prism, by attaching the additional Si atom face-capping on the pentagonal prism from the top, the side, or the upper inclined side. Isomers 11B, 11C, and 11D have higher energies than 11A by 0.29, 0.50, and 0.60 eV, respectively, and their calculated VDEs are 3.08, 3.12, and 3.18 eV, respectively. Thus, isomer 11A is considered as the most probable one detected in our experiments.

$CoSi_{12}^-$. The lowest-lying isomer of the $CoSi_{12}^-$ cluster is a D_{2d} symmetrical structure, which can be seen as a Si_2 dimer face-capping on the side of a distorted pentagonal prism. The calculated VDE of isomer 12A is 3.10 eV, which is in agreement with the experimental value (3.31 eV). The simulated spectrum of isomer 12A can well reproduce the positions, patterns, and intensities of the experimental spectrum. Both isomers 12B and 12D are a

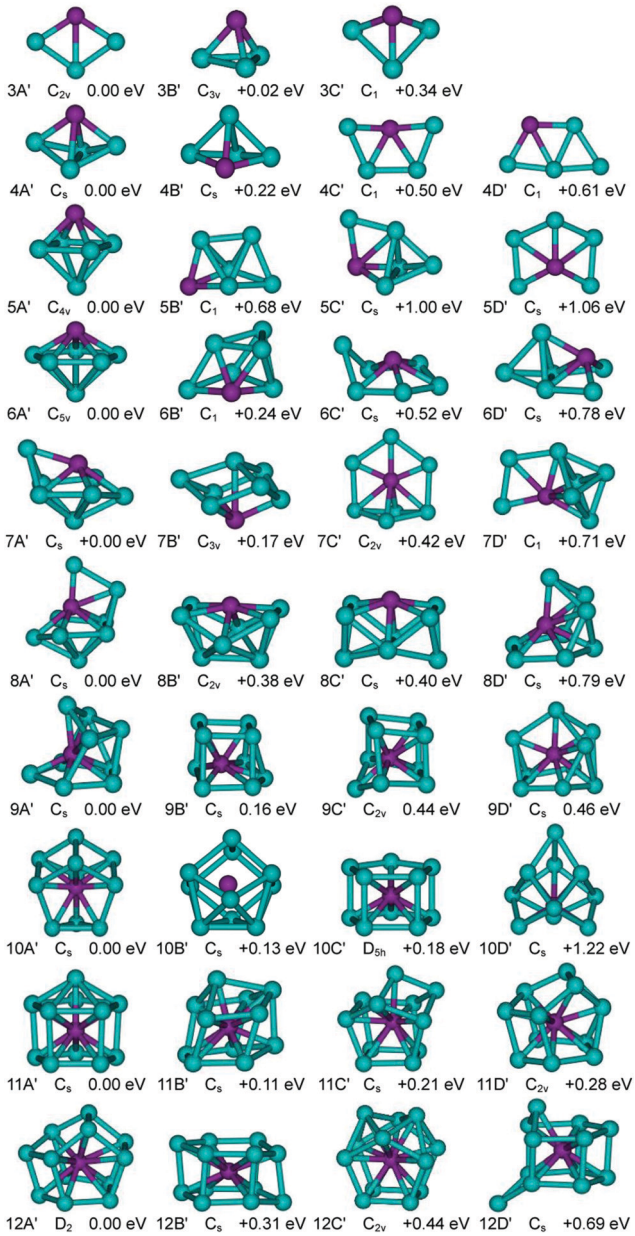

Fig. 4 Typical low-lying isomers of $CoSi_n$ (n = 3–12) clusters. The relative energies are calculated at the PBE/6-311+G(d) level. Purple and cyan balls stand for the Co and Si atoms, respectively.

distorted hexagonal prism. In addition, isomer 12C is derived from isomer 11D by adding one Si atom on the top. Isomers 12B, 12C, and 12D have higher energies than isomer 12A by 0.50, 0.50, and 1.09 eV, respectively. Therefore, the most probable isomer suggested in our experiments is isomer 12A.

Structures of neutral $CoSi_n$ (n = 3–12)

The structures of neutral $CoSi_n$ (n = 3–12) clusters are presented in Fig. 4. It is observed that the most stable structures of $CoSi_3$, $CoSi_8$, and $CoSi_{12}$ are similar to their anionic counterparts. The most stable isomer of $CoSi_4$ (4A′) is a trigonal bipyramid, similar to the second isomer of the $CoSi_4^-$ anion (4B). As for $CoSi_5$, the most stable structure (5A′) shows a resemblance with the second isomer of the $CoSi_5^-$ anion (5B), which is a square bipyramid. The lowest-lying structure of $CoSi_6$ (6A′) is a pentagonal bipyramid which is similar to isomer 6C. In the case of neutral $CoSi_7$, the most stable structure is similar to the fourth isomer of the $CoSi_7^-$ anion (7D). Similarly, for $CoSi_9$, the most stable structure is similar to the second isomer of the $CoSi_9^-$ anion (9B). The most stable structure of $CoSi_{10}$ has C_s symmetry while that of its anionic counterpart has C_{3v} symmetry. The most stable structure of $CoSi_{11}$ (11A′) is a pentagonal prism, showing similarity to isomer 11B of the $CoSi_{11}^-$ anion. It is worth pointing out that the most stable structures of neutral $CoSi_n$ (n = 3–12) clusters in our calculations are consistent with those reported by Wang *et al.*[30] with the only exception that their results showed that $CoSi_4$ has a planar structure and $CoSi_{10}$ has a pentagonal prism structure with Co at the center. The structures of $CoSi_{12}^{-/0}$ show huge difference from the hexagonal prism structures of $VSi_{12}^{-/0}$ (ref. 60) and $CrSi_{12}^{-/0}$,[61,62] and the reason may be that $CoSi_{12}^{-/0}$ cannot satisfy the 18-electron rule if we add up 9 valence electrons of cobalt with 12 electrons contributed by 12 silicon atoms.

Discussion

The dominant structures of $CoSi_n^{-/0}$ at small size for n = 3–6 are exohedral. The Co atom is half encapsulated into the silicon cage at n = 7. Starting from n = 10, the Co atom is completely encapsulated by the silicon cage. The structural evolution of $CoSi_n^-$ is somewhat similar to that of $CoGe_n^-$,[63] except that the geometric structures of $CoSi_n^-$ and $CoGe_n^-$ are slightly different from each other because the atomic radius of Ge is larger than that of Si and germanium is more metallic than silicon.

Fig. 5 shows the change of VDEs *versus* the number of silicon atoms, n. It can be seen that the VDEs increase as n increases from 3 to 10. The VDE value reaches a maximum (4.03 eV) at n = 10, and then decreases from 10 to 12. $CoSi_{10}^-$ has the highest VDE among the $CoSi_n^-$ clusters. It is also interesting to mention that $CoSi_{10}^-$ has the highest ion intensity among the $CoSi_n^-$ clusters, which can be observed from the mass spectrum of the current experiments (ESI,† Fig. S1). The high

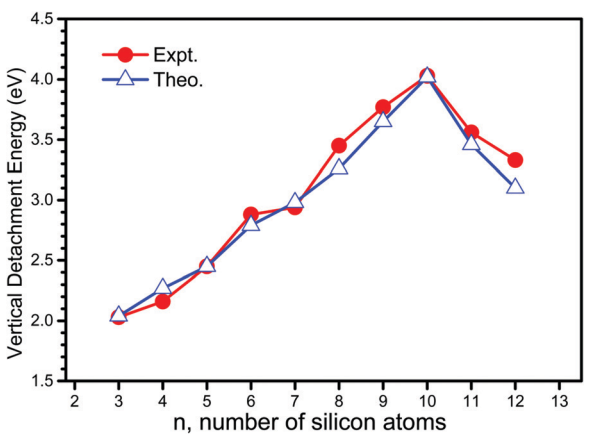

Fig. 5 Experimental and theoretical VDEs of $CoSi_n^-$ (n = 3–12) clusters *versus* n, the number of silicon atoms.

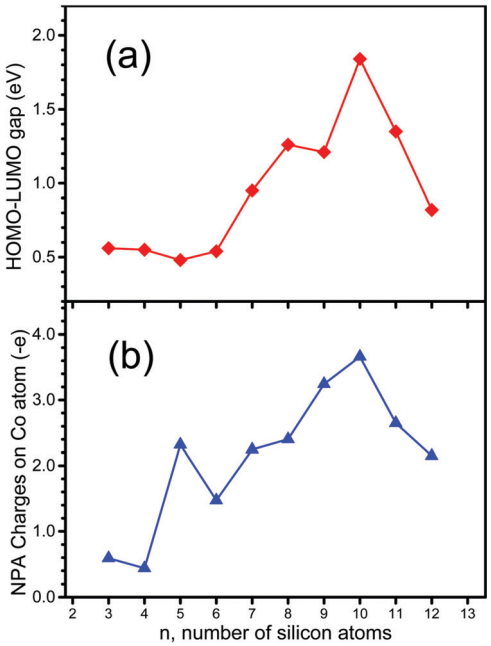

Fig. 6 (a) Size-dependence of the HOMO–LUMO gap of $CoSi_n^-$ (n = 3–12) clusters. (b) Size-dependence of NPA charges on the cobalt atom for $CoSi_n^-$ (n = 3–12) clusters.

VDE and high ion intensity of $CoSi_{10}^-$ are in agreement with formation of a C_{3v} symmetrical cage structure at n = 10. In addition, we investigated the gaps between the highest occupied molecular orbital and the lowest unoccupied molecular orbital (HOMO–LUMO gaps) for $CoSi_n^-$ (n = 3–12) clusters. The HOMO–LUMO gap *versus* n is shown in Fig. 6(a). It can be seen that $CoSi_{10}^-$ has the largest HOMO–LUMO gap. In addition, natural population analysis (NPA) for $CoSi_n^-$ (n = 3–12) clusters was also performed. The results of NPA charges on Co atoms are presented in Table 2 (NPA charges on Si atoms of $CoSi_{10}^-$ are presented in Table S1, ESI†) and Fig. 6(b). The negative charges on the Co atom increase as the number of Si atoms increases, reach a maximum at n = 10, and then decrease at n = 11–12. For $CoSi_{10}^-$, there are about −3.66 e charges on the Co atom, indicating some electrons transfer from the Si_{10} cage to the Co atom. From Table 2, one can see a loss of electrons in the Co 4s orbital and a gain of electrons in the Co 3d and 4p orbitals, suggesting there is hybridization among the Co 3d, 4s, and 4p orbitals. The Si atoms of $CoSi_{10}^-$ have electrons shared between the Si 3s and Si 3p orbitals, implying that there is hybridization between the Si 3s and 3p orbitals. The highest VDE value, largest HOMO–LUMO gap, and large electron density on the Co atom reveal that $CoSi_{10}^-$ has unusual stability.

To understand the electronic properties and stability of $CoSi_{10}^-$, we investigated its molecular orbitals in terms of the valence electrons as shown in Fig. 7. The valence electron configuration of the Co atom is $3d^74s^2$ and that of Si is $3s^23p^2$. $CoSi_{10}^-$ has a negative charge and the total number of valence electrons in $CoSi_{10}^-$ is 50. There are 25 molecular orbitals occupied by the valence electrons. It is interesting that the lowest orbital (HOMO−24) in Fig. 7 has a near-spherical shape which resembles an atomic 1s orbital. Above the lowest orbital, there are three orbitals degenerate in energy (HOMO−21, HOMO−22, and HOMO−23). The shapes of these degenerate orbitals are somewhat similar to atomic 2p orbitals. Similarly, in Fig. 7, some other molecular orbitals resembling atomic 3d, 2s, 4f *etc.* are observed. The shapes of these orbitals indicate that the valence electrons in $CoSi_{10}^-$ are strongly delocalized. Hence, it may be interpreted using the jellium model.[64–68] Based on the energy levels and the shapes of molecular orbitals in Fig. 7, we can tentatively write the jellium model electron configuration of $CoSi_{10}^-$ as $|1S^2|1P^6|1D^{10}|2S^21F^{14}|2P^62D^{10}$. This clearly shows that $CoSi_{10}^-$ has a closed-shell electron configuration according to the jellium model, in agreement with the stability of $CoSi_{10}^-$ observed in our experiments and theoretical calculations.

Table 2 NPA charges, total magnetic moments (μ_T), and natural electron configuration of the most stable isomers of $CoSi_n^-$ (n = 3–12) clusters

Cluster	NPA charge on the Co atom	μ_T [μ_B]	Natural electron configuration of the Co atom
$CoSi_3^-$	−0.591	2	$3d^{8.28}4s^{0.72}4p^{0.56}4d^{0.02}5s^{0.00}$
$CoSi_4^-$	−0.438	2	$3d^{8.37}4s^{0.54}4p^{0.47}4d^{0.03}5s^{0.00}$
$CoSi_5^-$	−2.321	0	$3d^{9.01}4s^{0.64}4p^{1.61}4d^{0.04}5s^{0.00}$
$CoSi_6^-$	−1.474	0	$3d^{8.84}4s^{0.48}4p^{1.09}4d^{0.04}5s^{0.00}$
$CoSi_7^-$	−2.246	0	$3d^{9.14}4s^{0.49}4p^{1.50}4d^{0.08}5s^{0.01}$
$CoSi_8^-$	−2.403	0	$3d^{9.17}4s^{0.52}4p^{1.61}4d^{0.07}5s^{0.01}$
$CoSi_9^-$	−3.244	0	$3d^{9.44}4s^{0.47}4p^{2.14}4d^{0.16}5s^{0.00}$
$CoSi_{10}^-$	−3.661	0	$3d^{9.60}4s^{0.05}4p^{2.27}4d^{0.33}5s^{0.40}$
$CoSi_{11}^-$	−2.649	0	$3d^{9.41}4s^{0.05}4p^{1.62}4d^{0.16}5s^{0.38}$
$CoSi_{12}^-$	−2.149	0	$3d^{9.31}4s^{0.36}4p^{1.26}4d^{0.10}5s^{0.06}$

It is also worth mentioning that the HOMO and HOMO−1 of $CoSi_{10}^-$ are degenerate in energy and fully occupied. Therefore, removal of one electron from the HOMO or HOMO−1 of $CoSi_{10}^-$ would induce Jahn–Teller distortion. It can explain why neutral $CoSi_{10}$ (C_s) has a lower symmetry than $CoSi_{10}^-$ (C_{3v}). Indeed, analysis of the molecular orbitals of neutral $CoSi_{10}$ (ESI,† Fig. S2) shows that the HOMO and HOMO−1 are split due to the Jahn–Teller effect. Li *et al.* analyzed the molecular orbitals and electron configuration of neutral $CoSi_{10}$ and interpreted the results based on the jellium model.[33] By comparing the molecular orbitals of $CoSi_{10}^-$ in the present work with those of the neutral $CoSi_{10}$ reported in the literature,[33] it is further confirmed that the degenerate molecular orbitals in $CoSi_{10}^-$ are split in neutral $CoSi_{10}$.

Conclusions

The structural evolution, and electronic and magnetic properties of the $CoSi_n^{-/0}$ (n = 3–12) clusters were explored using mass-selected anion photoelectron spectroscopy and quantum chemistry calculations. The critical size for the transition from an exohedral structure to an endohedral structure is n = 9 for the anions and n = 10 for the neutrals. The natural population analysis shows that the negative charges transfer from the silicon framework to the Co atom, and there is strong s–p–d hybridization in the interior of the Co atom. The magnetic moments of the Co atom are quenched when $n \geq 5$. The VDEs, ion intensities, NPA charges on the Co atom, and HOMO–LUMO gaps reach their maxima at n = 10. $CoSi_{10}^-$ has a C_{3v} symmetrical

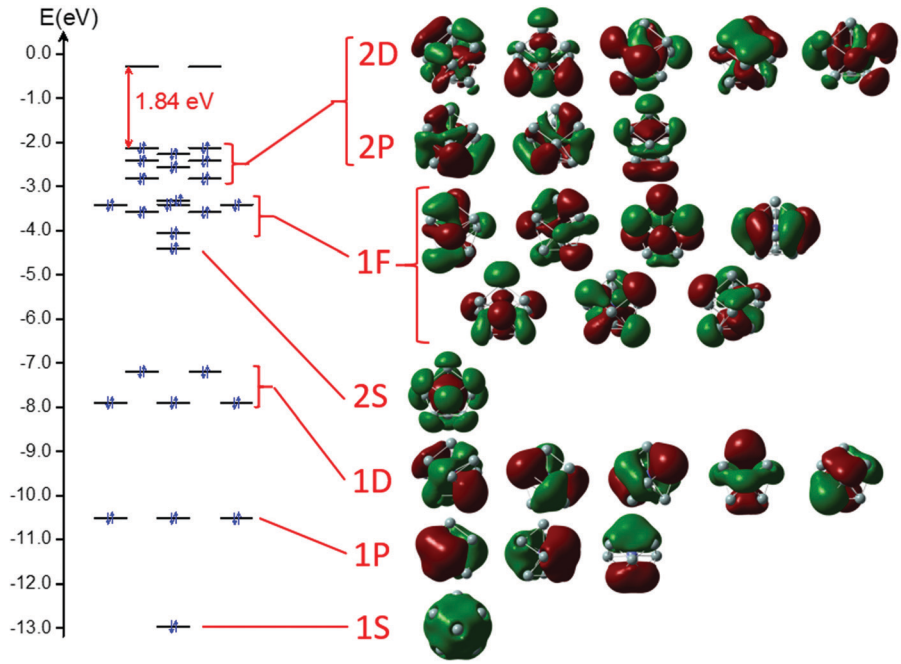

Fig. 7 Energy levels and diagrams of the molecular orbitals of $CoSi_{10}^{-}$.

tetracapped trigonal prism structure, and its special stability can be interpreted using the jellium model with a closed-shell electron configuration of $|1S^2|1P^6|1D^{10}|2S^21F^{14}|2P^62D^{10}$. As a result of Jahn–Teller distortion, the structure of neutral $CoSi_{10}$ has lower symmetry than its anionic counterpart.

Conflicts of interest

There are no conflicts of interest to declare.

Acknowledgements

This work was supported by the National Natural Science Foundation of China (Grant No. 21273246 and 21103202), the Chinese Academy of Sciences (Grant No. QYZDB-SSW-SLH024), the Beijing Municipal Science & Technology Commission (Grant No. Z181100004218004), and the Chinese Academy of Sciences President's International Fellowship Initiative (PIFI) (Grant No. 2018VMA0011). The theoretical calculations were performed on the China Scientific Computing Grid (ScGrid) of the Supercomputing Center, Computer Network Information Center of the Chinese Academy of Sciences.

References

1 S. M. Beck, *J. Chem. Phys.*, 1987, **87**, 4233–4234.
2 S. M. Beck, *J. Chem. Phys.*, 1989, **90**, 6306–6312.
3 M. Ohara, K. Koyasu, A. Nakajima and K. Kaya, *Chem. Phys. Lett.*, 2003, **371**, 490–497.
4 K. Koyasu, M. Akutsu, M. Mitsui and A. Nakajima, *J. Am. Chem. Soc.*, 2005, **127**, 4998–4999.
5 S. Neukermans, X. Wang, N. Veldeman, E. Janssens, R. E. Silverans and P. Lievens, *Int. J. Mass Spectrom.*, 2006, **252**, 145–150.
6 M. Akutsu, K. Koyasu, J. Atobe, K. Miyajima, M. Mitsui and A. Nakajima, *J. Phys. Chem. A*, 2007, **111**, 573–577.
7 S. Furuse, K. Koyasu, J. Atobe and A. Nakajima, *J. Chem. Phys.*, 2008, **129**, 064311.
8 A. Grubisic, H. Wang, Y. J. Ko and K. H. Bowen, *J. Chem. Phys.*, 2008, **129**, 054302.
9 P. Gruene, A. Fielicke, G. Meijer, E. Janssens, T. N. Vu, M. T. Nguyen and P. Lievens, *ChemPhysChem*, 2008, **9**, 703–706.
10 A. Grubisic, Y. J. Ko, H. Wang and K. H. Bowen, *J. Am. Chem. Soc.*, 2009, **131**, 10783–10790.
11 J. T. Lau, K. Hirsch, P. Klar, A. Langenberg, F. Lofink, R. Richter, J. Rittmann, M. Vogel, V. Zamudio-Bayer, T. Moller and B. Issendorff, *Phys. Rev. A: At., Mol., Opt. Phys.*, 2009, **79**, 053201.
12 H. G. Xu, Z. G. Zhang, Y. Feng, J. Y. Yuan, Y. C. Zhao and W. J. Zheng, *Chem. Phys. Lett.*, 2010, **487**, 204–208.
13 H. G. Xu, M. M. Wu, Z. G. Zhang, Q. Sun and W. J. Zheng, *Chin. Phys. B*, 2011, **20**, 043102.
14 V. Kumar and Y. Kawazoe, *Phys. Rev. Lett.*, 2001, **87**, 045503.
15 A. N. Andriotis, G. Mpourmpakis, G. E. Froudakis and M. Menon, *New J. Phys.*, 2002, **4**, 78.
16 S. N. Khanna, B. K. Rao and P. Jena, *Phys. Rev. Lett.*, 2002, **89**, 016803.
17 V. Kumar and Y. Kawazoe, *Phys. Rev. B: Condens. Matter Mater. Phys.*, 2002, **65**, 073404.
18 A. K. Singh, V. Kumar, T. M. Briere and Y. Kawazoe, *Nano Lett.*, 2002, **2**, 1243–1248.

19 J. Ulises Reveles and S. N. Khanna, *Phys. Rev. B: Condens. Matter Mater. Phys.*, 2006, **74**, 035435.
20 E. N. Koukaras, C. S. Garoufalis and A. D. Zdetsis, *Phys. Rev. B: Condens. Matter Mater. Phys.*, 2006, **73**, 235417.
21 J. G. Han, R. N. Zhao and Y. Duan, *J. Phys. Chem. A*, 2007, **111**, 2148–2155.
22 L. Z. Kong and J. R. Chelikowsky, *Phys. Rev. B: Condens. Matter Mater. Phys.*, 2008, **77**, 073401.
23 R. Robles, S. N. Khanna and A. W. Castleman, *Phys. Rev. B: Condens. Matter Mater. Phys.*, 2008, **77**, 235441.
24 J. Wang and J. H. Liu, *J. Phys. Chem. A*, 2008, **112**, 4562–4567.
25 R. Robles and S. N. Khanna, *Phys. Rev. B: Condens. Matter Mater. Phys.*, 2009, **80**, 115414.
26 G. F. Zhao, J. M. Sun, Y. Z. Gu and Y. X. Wang, *J. Chem. Phys.*, 2009, **131**, 114312.
27 R. N. Zhao, J. G. Han, J. T. Bai and L. S. Sheng, *Chem. Phys.*, 2010, **378**, 82–87.
28 A. H. Reader, A. H. Vanommen, P. J. W. Weijs, R. A. M. Wolters and D. J. Oostra, *Rep. Prog. Phys.*, 1993, **56**, 1397–1467.
29 L. Ma, J. Zhao, J. Wang, Q. Lu, L. Zhu and G. Wang, *Chem. Phys. Lett.*, 2005, **411**, 279–284.
30 J. G. Wang, J. J. Zhao, L. Ma, B. L. Wang and G. H. Wang, *Phys. Lett. A*, 2007, **367**, 335–344.
31 L. J. Guo, G. F. Zhao, Y. Z. Gu, X. Liu and Z. Zeng, *Phys. Rev. B: Condens. Matter Mater. Phys.*, 2008, **77**, 195417.
32 R. Robles and S. N. Khanna, *J. Chem. Phys.*, 2009, **130**, 164313.
33 Y. Li, N. M. Tam, P. Claes, A. P. Woodham, J. T. Lyon, V. T. Ngan, M. T. Nguyen, P. Lievens, A. Fielicke and E. Janssens, *J. Phys. Chem. A*, 2014, **118**, 8198–8203.
34 Y. J. Li, N. M. Tam, A. P. Woodham, J. T. Lyon, Z. Li, P. Lievens, A. Fielicke, M. T. Nguyen and E. Janssens, *J. Phys. Chem. C*, 2016, **120**, 19454–19460.
35 J. Chen, J. P. Colinge, D. Flandre, R. Gillon, J. P. Raskin and D. Vanhoenacker, *J. Electrochem. Soc.*, 1997, **144**, 2437–2442.
36 S. P. Chiu, S. S. Yeh, C. J. Chiou, Y. C. Chou, J. J. Lin and C. C. Tsuei, *ACS Nano*, 2017, **11**, 516–525.
37 T. H. Lin, T. Margossian, L. Q. Zheng, S. Kumar, I. Marozau, O. Sereda, D. Zemlyanov, C. J. Shih, R. Zenobi, D. Baudouin, G. De Micheli, P. E. Gaillardon and C. Copéret, *Chem. Mater.*, 2018, **30**, 2168–2173.
38 H. G. Xu, Z. G. Zhang, Y. Feng and W. J. Zheng, *Chem. Phys. Lett.*, 2010, **498**, 22–26.
39 J. Lv, Y. Wang, L. Zhu and Y. Ma, *J. Chem. Phys.*, 2012, **137**, 084104.
40 Y. C. Wang, J. Lv, L. Zhu and Y. M. Ma, *Comput. Phys. Commun.*, 2012, **183**, 2063–2070.
41 J. P. Perdew, K. Burke and M. Ernzerhof, *Phys. Rev. Lett.*, 1996, **77**, 3865–3868.
42 M. S. Gordon, J. S. Binkley, J. A. Pople, W. J. Pietro and W. J. Hehre, *J. Am. Chem. Soc.*, 1982, **104**, 2797–2803.
43 K. D. Dobbs and W. J. Hehre, *J. Comput. Chem.*, 1987, **8**, 861–879.
44 B. Yang, H. G. Xu, X. L. Xu and W. J. Zheng, *J. Phys. Chem. A*, 2018, **122**, 9886–9893.
45 G. D. Purvis and R. J. Bartlett, *J. Chem. Phys.*, 1982, **76**, 1910–1918.
46 G. E. Scuseria and H. F. Schaefer, *J. Chem. Phys.*, 1989, **90**, 3700–3703.
47 N. B. Balabanov and K. A. Peterson, *J. Chem. Phys.*, 2005, **123**, 064107.
48 D. E. Woon and T. H. Dunning, *J. Chem. Phys.*, 1993, **98**, 1358–1371.
49 M. J. Frisch, G. W. Trucks, H. B. Schlegel, G. E. Scuseria, M. A. Robb, J. R. Cheeseman, G. Scalmani, V. Barone, B. Mennucci, G. A. Petersson, H. Nakatsuji, M. Caricato, X. Li, H. P. Hratchian, A. F. Izmaylov, J. Bloino, G. Zheng, J. L. Sonnenberg, M. Hada, M. Ehara, K. Toyota, R. Fukuda, J. Hasegawa, M. Ishida, T. Nakajima, Y. Honda, O. Kitao, H. Nakai, T. Vreven, J. J. A. Montgomery, J. E. Peralta, F. Ogliaro, M. Bearpark, J. J. Heyd, E. Brothers, K. N. Kudin, V. N. Staroverov, T. Keith, R. Kobayashi, J. Normand, K. Raghavachari, A. Rendell, J. C. Burant, S. S. Iyengar, J. Tomasi, M. Cossi, N. Rega, J. M. Millam, M. Klene, J. E. Knox, J. B. Cross, V. Bakken, C. Adamo, J. Jaramillo, R. Gomperts, R. E. Stratmann, O. Yazyev, A. J. Austin, R. Cammi, C. Pomelli, J. W. Ochterski, R. L. Martin, K. Morokuma, V. G. Zakrzewski, G. A. Voth, P. Salvador, J. J. Dannenberg, S. Dapprich, A. D. Daniels, O. Farkas, J. B. Foresman, J. V. Ortiz, J. Cioslowski and D. J. Fox, *Gaussian 09, Revision A.02*, Gaussian, Inc., Wallingford, CT, 2009.
50 J. P. Foster and F. Weinhold, *J. Am. Chem. Soc.*, 1980, **102**, 7211–7218.
51 A. E. Reed, L. A. Curtiss and F. Weinhold, *Chem. Rev.*, 1988, **88**, 899–926.
52 J. E. Carpenter and F. Weinhold, *J. Mol. Struct.*, 1988, **169**, 41–62.
53 A. E. Reed, R. B. Weinstock and F. Weinhold, *J. Chem. Phys.*, 1985, **83**, 735–746.
54 A. E. Reed and F. Weinhold, *J. Chem. Phys.*, 1985, **83**, 1736–1740.
55 A. E. Reed and F. Weinhold, *J. Chem. Phys.*, 1983, **78**, 4066–4073.
56 F. Weinhold and J. E. Carpenter, *The structure of small molecules and ions*, Plenum, New York, 1988.
57 J. E. Carpenter, PhD thesis, University of Wisconsin-Madison, 1987.
58 D. J. Tozer and N. C. Handy, *J. Chem. Phys.*, 1998, **109**, 10180–10189.
59 J. Akola, M. Manninen, H. Häkkinen, U. Landman, X. Li and L. S. Wang, *Phys. Rev. B: Condens. Matter Mater. Phys.*, 1999, **60**, R11297–R11300.
60 X. M. Huang, H. G. Xu, S. J. Lu, Y. Su, R. B. King, J. Zhao and W. J. Zheng, *Nanoscale*, 2014, **6**, 14617–14621.
61 W. Zheng, J. M. Nilles, D. Radisic and K. H. Bowen, Jr., *J. Chem. Phys.*, 2005, **122**, 071101.
62 X. Y. Kong, H. G. Xu and W. J. Zheng, *J. Chem. Phys.*, 2012, **137**, 064307.
63 X. J. Deng, X. Y. Kong, X. L. Xu, H. G. Xu and W. J. Zheng, *ChemPhysChem*, 2014, **15**, 3987–3993.
64 W. Ekardt, *Phys. Rev. B: Condens. Matter Mater. Phys.*, 1984, **29**, 1558–1564.
65 A. W. Castleman and S. N. Khanna, *J. Phys. Chem. C*, 2009, **113**, 2664–2675.
66 P. Jena, *J. Phys. Chem. Lett.*, 2013, **4**, 1432–1442.
67 M. B. Abreu, A. C. Reber and S. N. Khanna, *J. Phys. Chem. Lett.*, 2014, **5**, 3492–3496.
68 O. C. Thomas, W. Zheng, S. Xu and K. H. Bowen, *Phys. Rev. Lett.*, 2002, **89**, 213403.